Environmental Pollution 399 (2026) 128160

Contents lists available at ScienceDirect

Environmental Pollution

journal homepage: www.elsevier.com/locate/envpol

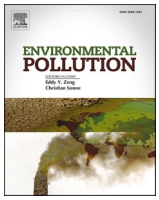

Environmental contamination with polystyrene micro and nano plastic affects *Mytilus galloprovincialis* ovaries

Rossana Romano [a,b,1], Vincenzo Migliaccio [c,*,1], Chiara Maria Motta [d], Luigi Rosati [d], Antonia Acquisto [d], Lillà Lionetti [c], Palma Simoniello [a,**]

[a] Department of Science and Technology, University of Naples Parthenope, 80143, Naples, Italy
[b] International PhD Programme, UNESCO Chair "Environment, Resources and Sustainable Development", Department of Science and Technology, University of Naples Parthenope, 80143, Naples, Italy
[c] Department of Chemistry and Biology "Adolfo Zambelli", University of Salerno, 84084, Fisciano, Italy
[d] Department of Biology, University of Naples Federico II, 80126, Naples, Italy

ARTICLE INFO

Keywords:
Oxidative stress
Apoptosis
Cytoskeletal proteins
Fibrosis
Protein glycosylation
Carbohydrate characterisation
Reproductive toxicology

ABSTRACT

Polystyrene micro- and nanoplastics (MNP) are persistent pollutants in aquatic environments worldwide. Once ingested, they accumulate in tissues and induce oxidative and cellular stress responses, leading to various adverse effects. However, their impacts on invertebrate reproductive systems remain poorly understood. In this study, we examined the effects of 5 μm microplastics (MP) and 0.1 μm nanoplastics (NP) on the ovaries of *Mytilus galloprovincialis*, a species commonly used as a bioindicator of coastal pollution. Both particles increased reactive oxygen species and lipid peroxidation while decreasing superoxide dismutase 2 expression. The redox imbalance was closely associated with significant changes in protein expression and cytoskeletal organisation. Disruption of vimentin and tubulin expression occurred alongside a displacement of cytosolic actin. Especially in ovaries exposed to NPs, these effects were accompanied by a markedly reduced oogonial proliferation and a higher rate of oocyte atresia. Caspase-3 activity and the BCL2 antagonist/killer Bak BAK expression corroborated these findings. Lectin-based analyses revealed significant changes in fucose, mannose, and N-acetylglucosamine residues in oocytes and adipogranular cells, confirming disturbances in protein glycosylation. Overall, the combined biochemical, structural, and molecular evidence suggests that both MP and NP severely disrupt oocyte maturation and diminish reproductive potential in *M. galloprovincialis*. Given mussels' ecological role as essential benthic filter feeders and sentinel organisms, these findings raise concerns about potential long-term impacts on population dynamics and coastal ecosystem resilience and highlight the urgent need for risk mitigation measures.

1. Introduction

Microplastics and nanoplastics (MNPs) are pollutants found in all aquatic environments, especially in densely populated areas such as coasts, rivers, and lakes (Talbot & Chang, 2022; Upendra & Kaur, 2023). Tides, winds, and currents aid in dispersal, and as a result, MNPs have reached even the most remote polar regions (Pellegrino et al., 2025).

Due to their small size, MNPs are easily mistaken for prey, especially by zooplanktonic organisms (Valdez-Cibrián et al., 2024), larvae (Ng et al., 2022), and filter feeders (Weber et al., 2021). Once ingested, particles cross the gut epithelium (Donkers et al., 2022) and, via circulation, reach different organs and tissues, accumulating (Habumugisha et al., 2024). The contaminated organisms are then preyed upon, spreading contamination throughout the food chain (Ziani et al., 2023).

In tissues, MNPs cause significant oxidative stress (Hu and Palić, 2020), activate the immune system (Lopez and Lamarre, 2025) and induce apoptosis (Xue et al., 2024). MNPs also alter DNA (Ernhofer et al., 2025), leading to genotoxicity (Shi et al., 2022) and cytotoxicity (Romano et al., 2025b).

MNPs also affect reproduction and gametogenesis (Yang and Wang, 2025). In particular, MNPs interfere with gonial recruitment and meiosis

* Corresponding author.
** Corresponding author.
E-mail addresses: vmigliaccio@unisa.it (V. Migliaccio), palma.simoniello@uniparthenope.it (P. Simoniello).
[1] The authors contributed equally.

https://doi.org/10.1016/j.envpol.2026.128160
Received 27 November 2025; Received in revised form 30 March 2026; Accepted 16 April 2026
Available online 21 April 2026
0269-7491/© 2026 The Authors. Published by Elsevier Ltd. This is an open access article under the CC BY-NC-ND license (http://creativecommons.org/licenses/by-nc-nd/4.0/).

progression, thus reducing fecundity (Pujol et al., 2025; Balali et al., 2024) and impairing fertilisation (Contino et al., 2023).

Despite the growing number of studies on MNP toxicity, the mechanisms underlying the distinct biological effects of microplastics and nanoplastics remain poorly understood. In particular, differences in their interactions with cellular structures, including their ability to penetrate tissues, interfere with cytoskeletal organisation, and affect specific organelles involved in gametogenesis, remain largely unexplored. Addressing these aspects is essential to better understand their impact on reproductive tissues (Yang et al., 2023).

This study examined the effects of 5 μm (MP) and 0.1 μm (NP) polystyrene beads on the ovaries of *Mytilus galloprovincialis*. Mussels are filter-feeding species; they inhabit highly contaminated inshore waters and, thereby, accumulate MPs and NPs in their tissues (Gagné et al., 2023). By adopting a comparative, multidisciplinary approach, we quantified oxidative stress and assessed the onset of associated fibrosis (An et al., 2021) by staining collagen with Picrosirius Red (Motta et al., 2024). The potential pro-apoptotic effects of MNP exposure were estimated by measuring changes in caspase-3 activity and Bak expression (Migliaccio et al., 2019) and by conducting cytohistological analyses of the resulting tissue damage. Particular attention was paid to the effects exerted on vinculin, tubulin, and actin. MNPs interfere with cytoskeletal components in vertebrate liver (Zheng et al., 2025), skin (Schmidt et al., 2023) and ovaries (Haddadi et al., 2022), but no information could be found for mussel oocytes. In parallel, we verified changes in the presence/distribution of carbohydrate residues, using fluorescent lectins Con A, UEA I, and WGA (Motta et al., 2022). Oogenesis is characterised by changes in sugar content (Motta et al., 2005), and polystyrene microplastics were reported to modify sugar residues present in yolk platelets n the crustacean *Artemia salina* (Motta et al., 2025).

2. Materials and methods

2.1. Animal care and treatments

Specimens of *Mytilus galloprovincialis* (average shell length: 6.60 ± 1.25 cm, n = 189 in total) were sourced from commercial suppliers during their reproductive season (December 2021 and March 2022; Rosati et al., 2019). They were maintained in 100 L tanks filled with artificial seawater (Instant Ocean Sea Salt, salinity 38 ± 1‰), at 18 ± 1 °C under a natural photoperiod (10 h light/14 h dark) as described by Motta et al. (2018) and fed marine zooplankton and phytoplankton formulated for aquarium use (Seachem Reef). An external pump connected to an oxygenator ensured proper water circulation and oxygenation. No biological or chemical filtration systems were used to avoid adsorption of microplastics (MPs) and nanoplastics (NPs) by filtering materials.

Mussel health was closely monitored, and no mortality was observed during the acclimation or exposure periods. Ethical approval was not required for this species; however, all procedures were conducted in accordance with animal welfare principles, minimising stress and the number of animals used.

After 5 days of acclimation, mussels (n = 63 per triplicate experiment) were randomly divided into three groups of 21 animals: control, MP exposure, or NP exposure. Each group was further split into three subgroups of 7 animals, which were randomly allocated to 20 L polycarbonate tanks (Motta et al., 2018). Exposures lasted for 1, 3, or 11 days. During the first two, water was not replaced, whereas for the 11-day exposure, the water was replaced entirely on day 5.

Polystyrene MPs (5 μm; 1×10^7 particles/mL) and NPs (0.1 μm; 1×10^9 particles/mL; 0.55 μg/L) were obtained from Thermo Scientific™ (Duke Standards™ 2000 Series Uniform Polymer Particles). For the treatments, the particles, in distilled water, were diluted to the environmentally realistic concentrations of 1×10^2 particles/mL for MPs (6.8 μg/L polystyrene; Leusch & Zijahromi, 2021; Vroom et al., 2017) and 2.2×10^4 particles/mL for NPs (0.012 ng/L polystyrene; Leusch & Zijahromi, 2021; Capolupo et al., 2021).

2.2. Oxidative stress parameters

To test the pro-oxidant effect of PS-MNPs, gonadal tissue was homogenised in cold-ice lysis buffer (50 mM Tris, pH 7.4, 150 mM NaCl, 1 mM EDTA, 1% Triton X-100).

ROS levels were measured by monitoring the ROS-induced conversion of 2′,7′-dichlorodihydrofluorescin diacetate (DCFH-DA, a non-fluorescent compound) into dichlorofluorescein (DCF, a fluorescent compound), as reported by Driver et al. (2000). Homogenate aliquots containing 25 μg of protein were incubated in 200 μl of 0.1 M monobasic phosphate buffer, pH 7.4, for 15 min in the presence of 10 μM DCFH-DA. $FeCl_3$ was added to achieve a final concentration of 100 μM; the mixture was then incubated for 30 min. A 96-well plate reader was used to detect the conversion of DCFH-DA to the fluorescent product DCF (λ_{ex} 485 nm, λ_{em} 530 nm). The conversion of DCFH to DCF in the absence of gonadal homogenate served as a background fluorescence control. A standard curve of DCF was utilised to calculate nmol DCF formed.

Oxidative damage to lipids was measured spectrophotometrically by assessing TBAR levels in total tissue homogenates, following the method described by Aguilar Diaz de Cerio et al. (2020). Briefly, homogenates containing 0.5 mg of protein were incubated with thiobarbituric acid solution at pH 4 and heated at 95 °C for 1 h. The samples were then centrifuged and read at 535 nm using a microplate reader. A standard curve of malondialdehyde (MDA), the final product of lipid peroxidation, was used for quantification.

2.3. Protein extraction, electrophoresis and gel staining

Gonadal fragments were washed with PBS 1x and lysed in cold-ice lysis buffer solution (50 mM Tris pH 7.4, 150 mM NaCl, 1 mM EDTA, 1% NP40) supplemented with phosphatase inhibitors (2 mM NaOVa, 100 mM NaF, 20 mM NaPPi), deacetylase inhibitors (5 mM Nicotinamide, 1 mM Na-butirrate), and protease inhibitors cocktail (Roche; 1 tablet per 10 mL of lysis buffer). The lysate obtained was centrifuged at 12000×*g* for 10 min. The protein content of the resulting supernatant was quantified by using the Pierce BCA Protein Assay Kit (Thermo Scientific).

About 35 μg proteins were denatured in 2x loading buffer (final concentration: 120 mM Tris HCl, pH 6.8, 20% glycerol, 4% SDS and 0,05 mM DTT) at 95 °C and loaded onto a SDS-polyacrylamide gel together with prestained protein markers (Spectra Multicolour Broad Range Protein Ladder, 10,000–240,000 Da). After running, proteins were stained with Coomassie blue.

To detect glycosylated proteins, unstained gels were incubated in 0.5% periodic acid for 15 min, washed in distilled water, and stained with Schiff reagent for 5 min in the dark. Gels were destained in 0.5% sodium metabisulfite until bands appeared clearly.

2.4. Western Blot analyses

Unstained gels were transferred to a PVDF membrane (Immobilon-P, Millipore, 0,45 μm, Schwerzenbach, Switzerland) at 350 mA for 60 min.

The membranes were blocked in blocking buffer solution (BBS; 1% Tween-20, 5% milk in 1x PBS) for 60 min at room temperature and incubated overnight at 4 °C with the antibody of interest. On the second day, the membranes were washed in 1% Tween-20 in 1x PBS and incubated for 1 h at room temperature with the secondary antibodies diluted 1:10000 in BBS. 1x PBS/1% Tween-20, 5% milk. After washing in 1% Tween-20 in 1x PBS, the labeled proteins were detected with the ECL system (Amersham ECL Western Blotting Detection Reagent) using the iIBright 1500 (Thermo Fisher Scientific) system. Densitometric analysis of band intensities was performed using the ImageJ software (version 1.54p, released February 18, 2025) and normalized to the corresponding internal control GAPDH.

Primary antibodies used for analyses were: Bak (sc-517390, Santacruz biotech, 1:1000); SOD2 (#PA5-30604, Invitrogen, 1:1000); vinculin (NBP1-47065, Novus Biological, 1:1000); tubulin (ab4074, Abcam, 1:2000). GAPDH (14952382, Invitrogen, 1:1000) was used as loading control of proteins in each sample. Secondary antibodies were peroxidase-conjugated anti-rabbit and anti-mouse (Peroxidase-Affini Pure Donkey, Biorad Laboratories) diluted 1:10000.

2.5. Caspase 3 activity detection

To detect apoptosis, the Caspase 3 Assay Kit, Colourimetric, from Sigma-Aldrich (CASP3C-1 KT) was used. Sample preparation and test were performed as indicated by the manufacturer. Briefly, 10 μL of gonad lysates were incubated in 1X assay buffer in the presence of the caspase 3 substrate acetyl-Asp-Glu-Val-Asp p-nitroanilide (Ac-DEVD-pNA). The hydrolysis of the substrate by caspase 3 results in the release of p-nitroaniline (pNA), which turns the buffer yellow. pNA absorbance was read at 405 nm. The absorbance of pNA was normalized with protein content in each sample. To calculate the pNA concentration in samples, a calibration curve prepared with pNA standards was used.

2.6. Histological analyses

a) *Section preparation.* Gonad samples (n = 3 per treatment per triplicate experiment) were collected at different exposure times, fixed in Bouin's (24 h), and embedded in paraffin according to standard protocols (Simoniello et al., 2010). Sections of 5 μm were stained with Haemalum-Eosin to show the general morphology or with Mallory trichrome (modified according to Galgano) to show cytoskeletal details (Motta et al., 2018).
b) *Collagen staining.* Collagen deposition was highlighted by Picrosirius red staining (Rosati et al., 2023). Paraffin sections were deparaffinized, rehydrated through a graded ethanol series, and stained with 0.1% Sirius Red F3B (Direct Red 80, Sigma-Aldrich, Milan, IT) in a saturated aqueous picric acid solution for 1 h at room temperature. Sections were then washed twice in acidified water (0.5% acetic acid) to remove unbound dye, dehydrated rapidly in absolute ethanol, cleared in xylene, and mounted in DPX. Slides were observed under bright and UV light. All images were acquired using a Zeiss Axiocam camera mounted on a Zeiss Axioskop microscope (Zeiss, Jena, Germany).
c) *F-Actin Staining.* Actin filaments were detected by staining with Texas Red©- X phalloidin (Molecular Probes Invitrogen Detection Technologies, Eugene, Oregon, USA; 5 μL diluted into 200 μL PBS). All images were acquired using a Nikon Eclipse E200 and a Nikon Eclipse Ni-U.
d) *Lectin staining.* Sugar residues were characterised by staining with FITC-conjugated lectins (Vector Laboratories Inc., Newark, CA, USA; 2 μl diluted in 50 μl PBS pH 7.4; Motta et al., 2022). Negative controls were prepared by omitting the lectin (to check for tissue autofluorescence) or by co-incubating the slides with the lectin and the specific competing sugar to verify lectin-binding specificity. Two independent observers assessed labelling intensity. Lectins used were DBA (*Dolichos biflorus* agglutinin) for N-acetyl-galactosamine (galNAc) and PNA (*Arachis hypogaea* agglutinin) for terminal galactose (gal) (Fogliano et al., 2023). Images were acquired using a Nikon Eclipse E200 and a Nikon Eclipse Ni-U.

2.7. Immunohistochemistry

Sections mounted on polylysine glass slides were treated with 10 mM citrate buffer, pH 6.0, to unmask antigens and incubated in 2.5% H_2O_2 in methanol to block endogenous peroxidase (Agnese et al., 2013). Non-specific signals were reduced by incubation in normal goat serum for 1 h at room temperature. Slides were incubated overnight at 4 °C with a primary rabbit anti-human PCNA antibody (Elabscience, Bionovation Inc., Rome, IT) at a 1:300 dilution.

The next day, the sections were incubated with HRP-conjugated goat anti-rabbit secondary antibody diluted 1:200 in normal goat serum for 1 h at room temperature, followed by incubation with an avidin-biotin-peroxidase complex (ABC Immune Peroxidase Kit, Pierce) for another 1 h at room temperature. Finally, the sections were stained with diaminobenzidine as chromogen and counterstained with Meyer's haematoxylin. Negative controls were obtained by omitting incubation with the primary antibody. The reaction was observed using a Zeiss Axioskop microscope, and images were acquired with a Nikon Eclipse Ni-U microscope and a Nikon DS-F*i*3 camera.

2.8. Analysis of data

After FITC-phalloidin, FITC-lectin and picrosirius red staining, fluorescence intensity was evaluated by ImageJ (free version 1.54p, updated 17 February 2025). Random digital photos (20 × magnification; n = 10 per treatment) were converted to high-resolution (400 dpi), 8-bit, 256-grayscale TIFF images. Density values, determined in n = 75 square areas/treatment, were pooled and reported as a percentage of the respective control values.

Band intensity for PAS and Coomassie gels staining was evaluated using GelAnalyzer 23.1.1 (available at www.gelanalyzer.com) by Istvan Lazar Jr., PhD and Istvan Lazar Sr., PhD, CSc.

After checking the normal distribution of the data using the Shapiro–Wilk test (Migliaccio et al., 2024), significance of treatments was assessed using the Student's t-test, or one-way ANOVA, followed by a Tukey's pairwise comparison test. Statistical analyses were performed with GraphPad Prism 9.0 Software (San Diego, CA, USA). The minimum level of significance accepted was $p < 0.05$ (*).

3. Results

3.1. Effects of MNP exposure on oxidative balance and stress

Analyses of total gonadal lysates showed that ROS levels increased up to 2.6-fold compared to controls after exposure to MPs for 11 days. NPs exposure resulted in an even more significant increase of 3.3-fold at 1 and 11 days, and 3.7 times at 3 days (Fig. 1A).

A time-dependent increase in lipid peroxidation was also observed (Fig. 1B). MP-treated samples showed a progressive increase of 1.9-, 2.1-, and 2.6-fold at 1, 3, and 11 days, respectively. NP exposure resulted in even higher levels with 2.3-, 2.5-, and 2.9-fold increases at the same time points (Fig. 3B). No significant differences in ROS and lipid peroxide levels were observed between MPs- and NPs-treated groups.

Oxidative stress was associated with alterations in Mn/SOD2, a key mitochondrial antioxidant enzyme and marker of cellular defence (Fig. 1C and D). After 1 day of exposure, SOD_2 levels increased by approximately 1.6 times in MP-treated and 2 times in NP-treated ovaries compared to controls. In contrast, exposure for 3 and 11 days led to significant reductions. Specifically, MPs reduced SOD_2 levels by about 50% at both time points, while NPs caused a downregulation of approximately 45% at 3 days and 73% at 11 days.

3.2. Effects of MNP on protein pattern and protein glycosylation

Exposure to MNPs resulted in significant time-dependent changes in protein patterns, with variations in band presence and intensity. After 1 day of exposure, MP and NP resulted in a 15% and a 53% decrease in the band at ~130 kDa, while a 68% and a 16% increase occurred in the band at ~120 kDa. Moreover, significant decreases of about 16% and 32% were observed for bands of about 20 kDa in MP and NP, respectively. In MP, a series of bands also appeared between ~60 and 80 kDa (Fig. 2A–A').

At 3 days, MP exposure caused significant changes in the mid-to low-molecular-weight range. In MP samples, two new bands appeared at

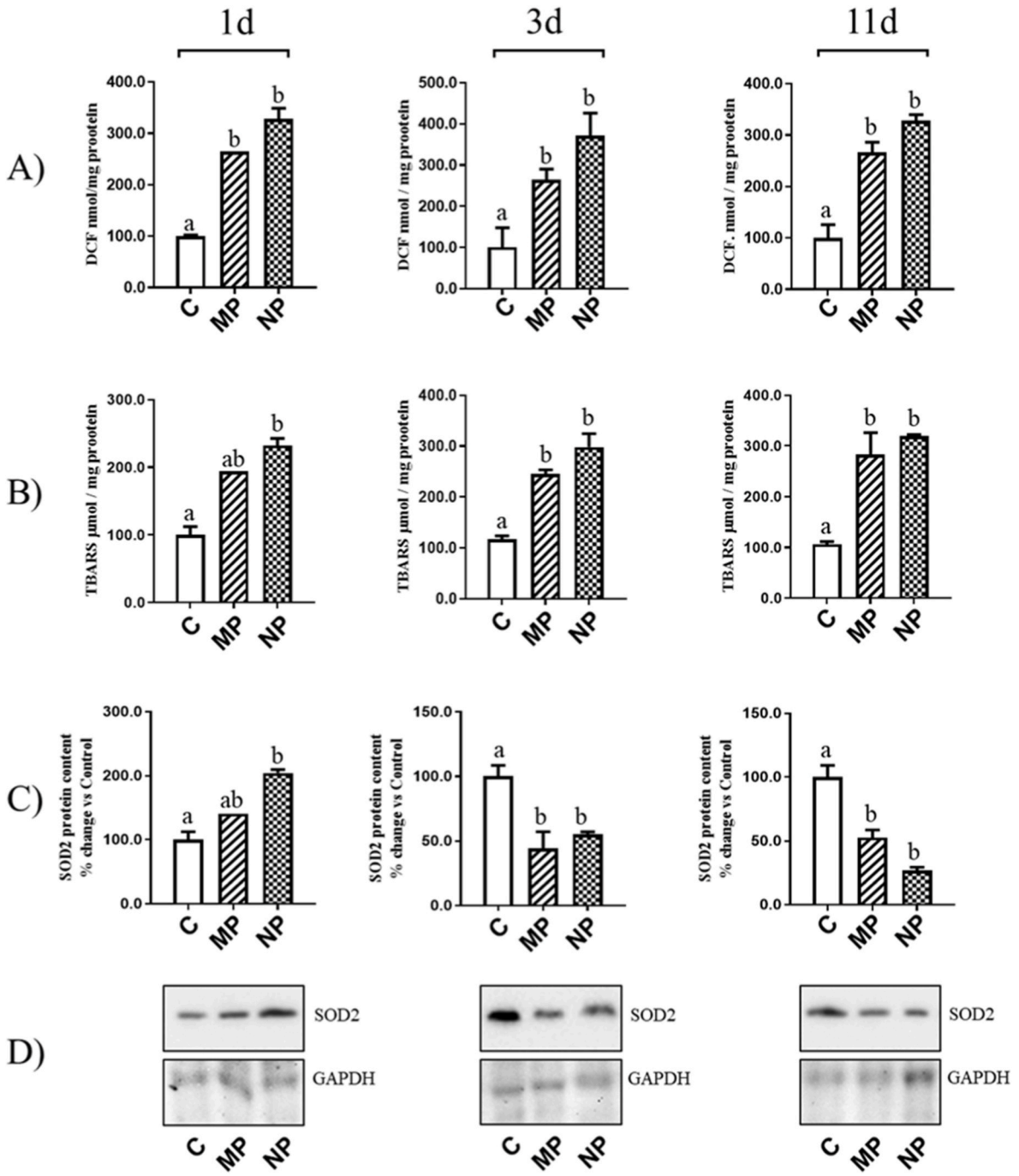

Fig. 1. Effects of MPs and NPs exposure for 1, 3, or 11 days on oxidative stress parameters. Total ROS (A), lipid peroxides (B), and SOD_2 expression (C). Representative Western blot for SOD_2 and the loading control GAPDH (D). Data are means ± SEM. (One-way ANOVA; different letters indicate statistically significant differences at $p < 0.05$).

~45 kDa and ~22 kDa. A generalised decrease in protein band number and/or intensity was observed in NPs (Fig. 2B–B'). After 11 days, there was a noticeable decrease in the 60-100 kDa bands, accompanied by an increase in bands at 40–50 kDa. A ~20 kDa band appeared in MPs, whereas in NP, the ~45 kDa band increased in intensity (Fig. 2C–C').

Exposure to MNPs also caused time-dependent changes in protein glycosylation. On day 1, in MPs samples, bands between ~40 and 130 kDa appeared more intense, while in samples exposed to NPs, the band at ~50 kDa significantly decreased in intensity (Fig. 2D–D').

At 3 days, in MPs, the band at ~50 kDa remained intense, whereas bands at higher molecular weights were not. In contrast, NPs showed increased glycosylation between ~60 and 130 kDa (Fig. 2E–E'). By day 11, bands between ~60 and 130 kDa lost glycosylation, while proteins around ~40–50 kDa displayed increased glycosylation, especially in NPs (Fig. 2F–F').

3.3. Cytoskeletal protein modifications following MNP exposure

No significant changes in vinculin (Fig. 3A–C) were observed compared to controls at any point after MP exposure. No change was observed in the NPs samples at 1 day. In contrast, at 3 and 11 days, the expression decreased to one-third and increased by 1.4-fold, respectively.

Following MP exposure, tubulin (Fig. 3B and C) remained unchanged

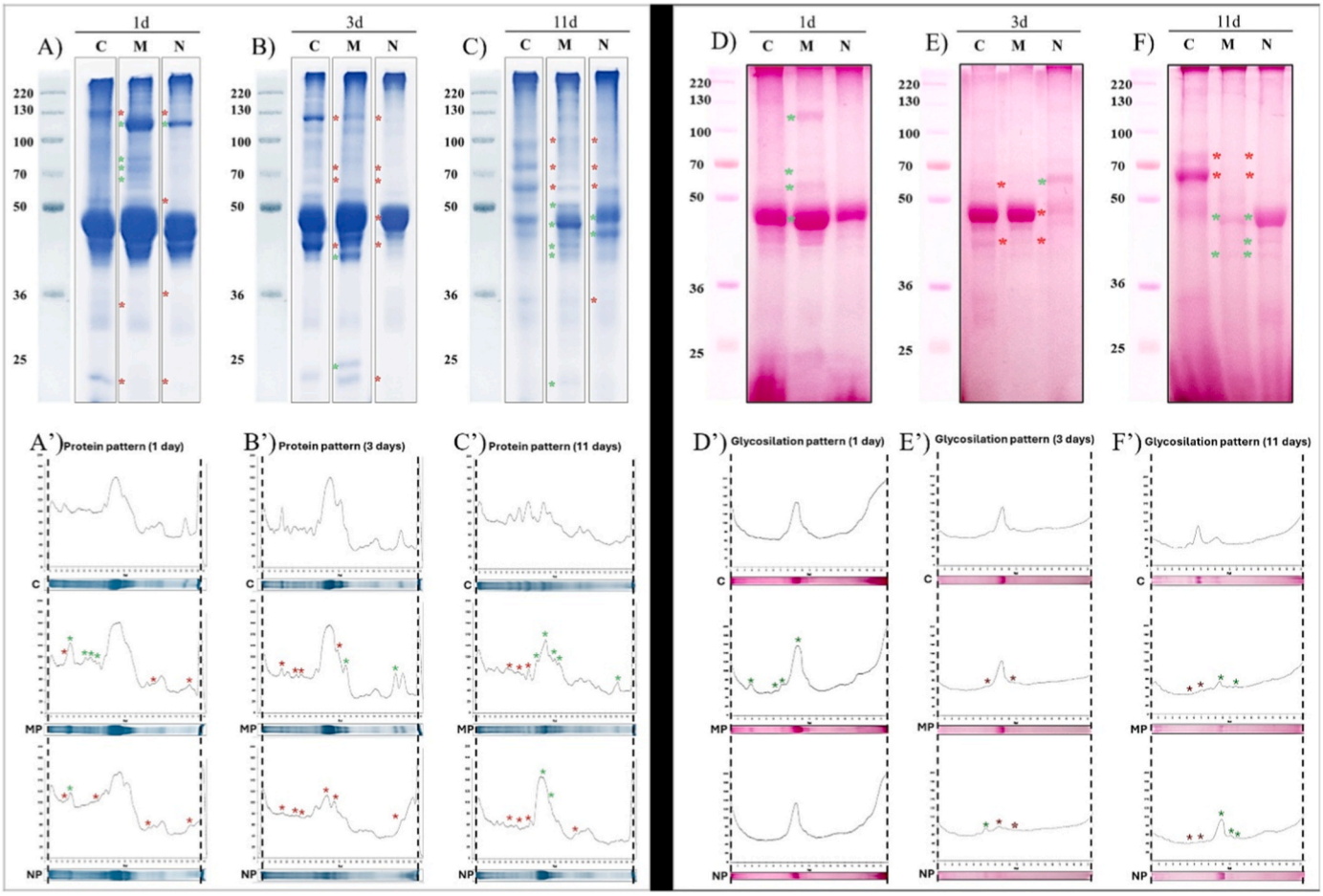

Fig. 2. Effects of MP and NP exposure for 1, 3, or 11 days on gonadal total protein extracts. (A–C) Coomassie-stained gels and (A′-C′) corresponding relative protein band intensities. Protein glycosylation profiles are shown in (D-F) PAS-stained gels and (D′-F′) the corresponding relative band intensities. Red and green asterisks indicate bands with decreased or increased intensity, respectively. Protein band intensities determined with GelAnalyzer 19.1. (For interpretation of the references to colour in this figure legend, the reader is referred to the Web version of this article.)

at 1 day, and increased 2.3-fold at 3 days, and 9.3-fold at 11 days. In NP-treated samples, tubulin rose 2.3-fold on day 1 and 3.3-fold on day 11, decreasing to about one third on day 3.

At the cytological level, changes in the cytoskeleton were confirmed by notable alterations in the oocyte cytoplasm. After staining with FITC-phalloidin, in control ovaries, the F-actin was concentrated around the yolk platelets, thus giving the cytoplasmic fluorescence a granular appearance (Fig. 3D). Following exposure to MNP, from day 3 onwards (Fig. 3E), the labeling gradually dispersed and fluorescence evenly spread across the entire cytoplasm (Fig. 3F). Quantitative analyses confirmed the dispersion of actin into the cytoplasm, with more pronounced effects on fluorescence levels observed for MP at 11 days of exposure (Fig. 3G).

3.4. Effects of MNP exposure on apoptosis and cell proliferation

Results showed a time-dependent increase in caspase-3 activity (Fig. 4A–C) and BAK expression (Fig. 4B andC). Specifically, in MP samples, the activity rose 17-fold on day 3 and 24-fold on day 11. Bak expression increased 3-fold on both day 3 and day 11. No effects were observed on day 1. In contrast, NPs activated caspase 3 as early as day 1 with a 2.7-fold increase, and the effect grew stronger on days 3 and 11, reaching a 20-fold increase. Bak showed a 2-fold rise on days 1 and 3, and a 2.5-fold increase on day 11.

In control samples (Fig. 4D), in samples exposed to MPs (Fig. 4E), and in those exposed to NPs for 1 or 3 days (data not shown), proliferating nuclear antigen PCNA was localised in the nuclei of proliferating oogonia and early-growing oocytes. In larger oocytes, the nuclei showed a reduced labeling while an intense perinuclear staining was observed (Fig. 4E inset). No difference was noticed between healthy and atretic oocytes (Fig. 4E and F). In the NPs samples exposed for 11 days (Fig. 4F), no differences were observed in large oocytes with respect to control. The small oocytes, located into or close to the connective wall, were always unstained. In all samples, occasional adipogranular (Fig. 4D) but not vesicle cells (Fig. 4E) showed positivity.

3.5. Effects of MNP exposure on ovarian follicle morphology

In controls, approximately half of the ovaries were in the peri-ovulatory stage (Fig. 5A), characterised by follicles filled with mature eggs. Few atretic oocytes exhibited dense cytoplasm. The mantle contained large vesicular connective cells (VCT), whereas the adipogranular cells (ADG) were reduced in size. The other half of the ovaries was between the post-ovulatory phase (follicles nearly empty; Fig. 5B) and the early growth phase (Fig. 5C). The latter contained early-growing oocytes often in contact with small, hypertrophic ADG cells (Fig. 5D). No significant differences were observed among days 1, 3, and 11 (Fig. 5P).

On day 1, in mussels exposed to MPs, follicles showed an increased number of atretic oocytes. As in controls, they displayed a moderately altered shape and clear cytoplasm (Fig. 5E). In contrast, on days 3 and 11, the number of atretic follicles increased (Fig. 5P) and, most relevant, they contained altered oocytes, with sparse residues in the lumen

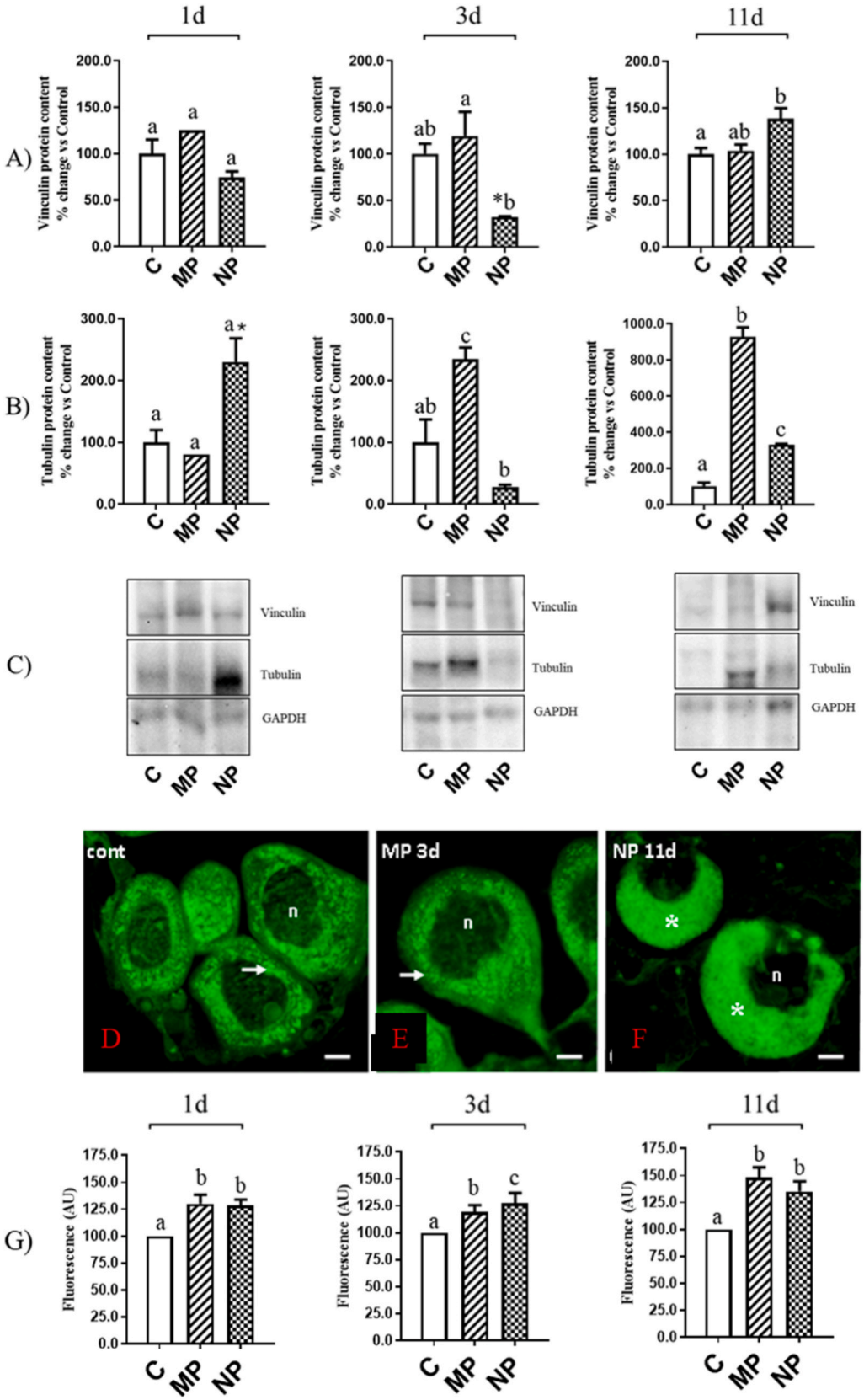

Fig. 3. Cytoskeletal proteins vinculin (A, C), tubulin (B, C), and actin (D-G) in ovaries exposed to MPs or NPs for 1, 3, or 11 days. (A-B) Quantitative analysis of protein expression. (C) Representative Western blots for vinculin, tubulin, and the loading control GAPDH. (D-F) Representative images of actin dispersal within the oocyte cytoplasm. Actin surrounding yolk globules (arrow) or spread in the cytosol (*); nuclei (n). Staining with FITC-phalloidin; bars 5 μm. (G) Quantification of oocyte fluorescence using ImageJ (free version 1.54p, updated 17 February 2025). Data are means ± SEM for WB data or SD for fluorescence intensities. Different letters indicate statistically significant differences determined by ANOVA ($p < 0.05$). Asterisks (*) denote significant differences according to Student's t-test ($p < 0.05$). Fig. 3

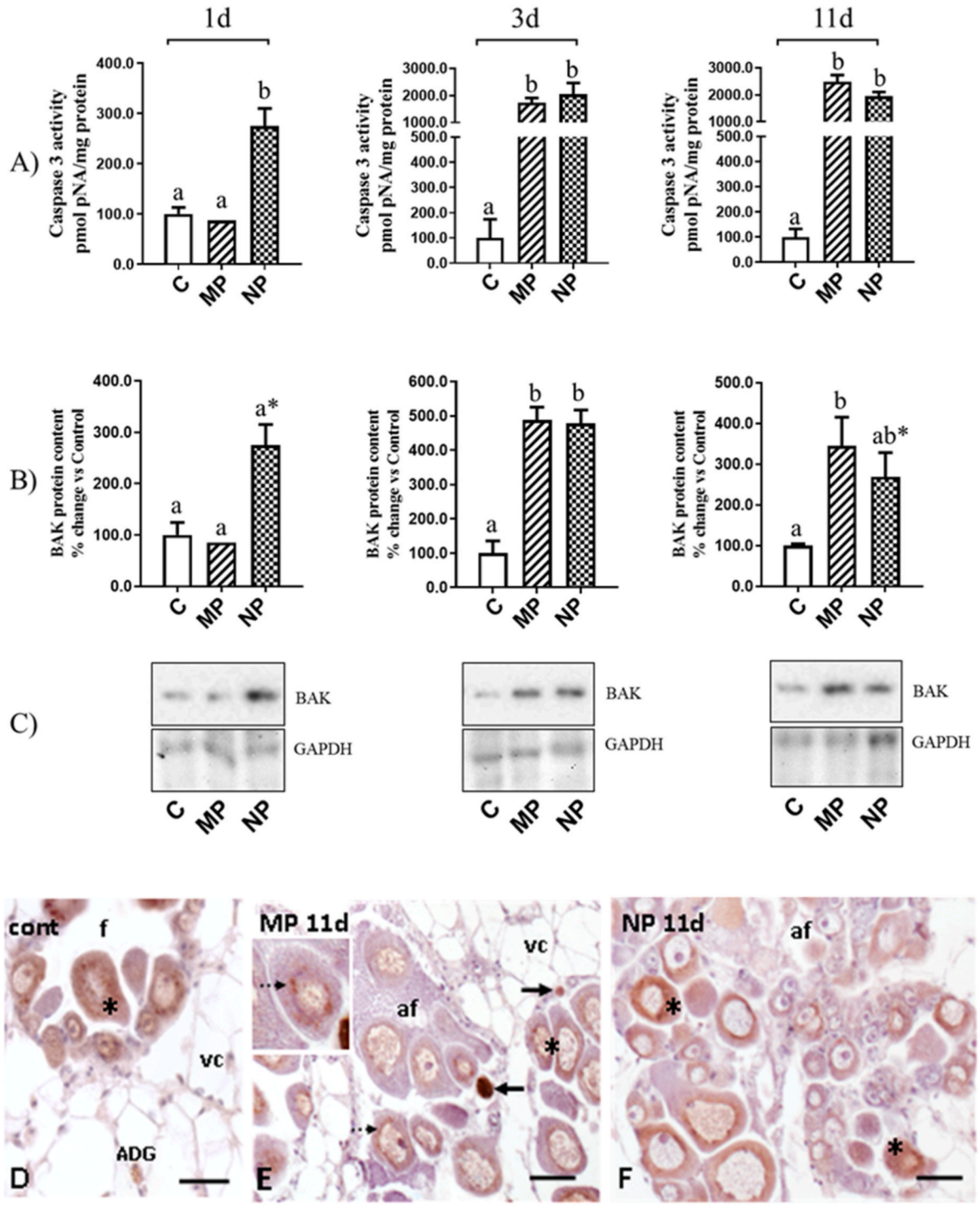

Fig. 4. Apoptosis and proliferation markers in ovaries exposed to MPs or NPs for 1, 3, or 11 days. (A-B) Quantitative analysis of caspase 3 activity and BAK expression. (C) Representative Western blots for BAK and the loading control GAPDH. Data are means ± SEM. Different letters indicate statistically significant differences determined by ANOVA ($p < 0.05$). Asterisks (*) denote significant differences according to Student's t-test ($p < 0.05$). (D-F) Localisation of PCNA antigen in representative control (D), MP (E) and NP (F) samples. Ovarian follicle (f), atretic follicle (af), adipogranular cell (adg), vesicular cells (vc). Labeling on the nucleus (arrow), cytoplasm (*) or perinuclear cytoplasm (dotted arrows). In F) notice the absence of nuclear labeling (double arrow) in small oocytes. Mild counterstain with haemalum; bars: 50 μm.

(Fig. 5F). At higher magnification, apparently healthy oocytes showed large, clear areas in the cortical cytoplasm (Fig. 5K) and/or dense treads forming a sort of cytosolic net (Fig. 5M). The nuclei displayed indented contours and occasional dense patches of chromatin (Fig. 5L), features not observed in control oocytes (Fig. 5D). In the connective tissue, from day 3, dispersed haemocytes increased and patches of inflammatory tissue became common (Fig. 5I).

Following the NPs' exposure, marked alterations were observed from day 1 (Fig. 5P). The follicles mostly contained atretic oocytes and abundant dispersed residual material (Fig. 5G). Haemocyte infiltration was relevant in both the follicular lumen (Fig. 5H) and the connective tissue (Fig. 5J). Higher magnification confirmed the occurrence of

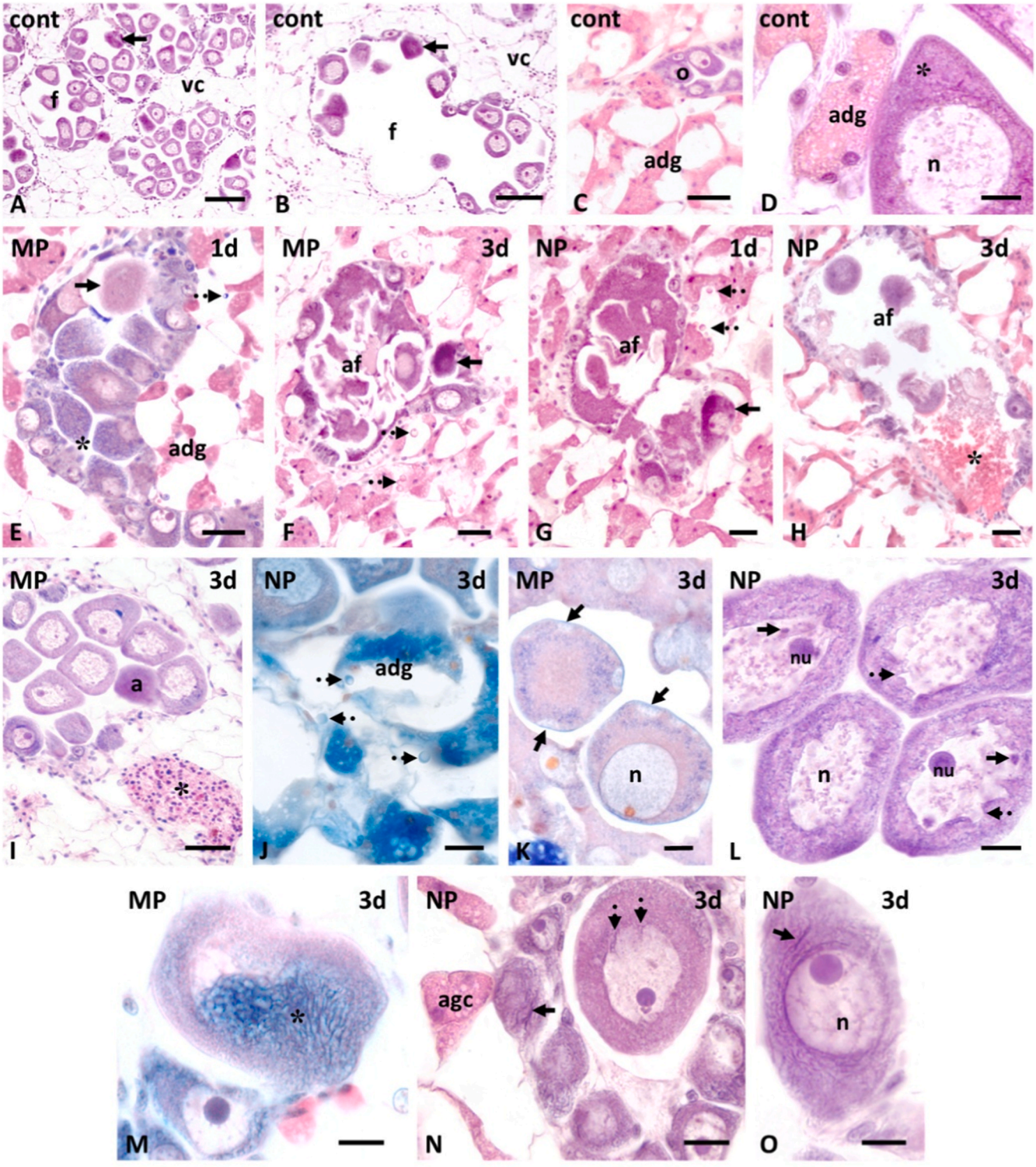

P		CONTROL			MPs			NPs		
	observations/treatment	1d	3d	11d	1d	3d	11d	1d	3d	11d
follicle degeneration	n ≥ 90 follicles	-	-	±	±	+	++	++	±	±
inflammation	n = 9 animals	-	-	-	-	±	+	-	+	+++
altered cortical cytoplasm	n ≥ 180 oocytes	-	-	-	±	-	+	±	-	++
altered cytoskeleton	n ≥ 180 oocytes	-	-	±	±	±	+	-	-	++
indented nuclear contour	n ≥ 180 oocytes	-	-	-	-	+	+++	-	±	++

(caption on next page)

Fig. 5. Alterations in ovaries exposed to MPs or NPs for 1, 3, or 11 days. Representative images of control (A-D) ovaries and damage in exposed ovaries (E-O), with relative frequencies (table). Pre (A) and early post (B) follicles (f) containing mature eggs (e), atretic oocytes (arrows). Vesicular cells (vc) in the connective tissue. C) Early growing follicles with oogonia and early oocytes (o). D) Detail of contact between oocyte and adg cells. E) Growing early oocyte (arrow) with occasional atretic oocytes (oocyte). Dense cytoplasm (*); haemocyte (dotted arrow). F-G) Altered follicles (af) showing abundant dispersed materials. Atretic oocyte (arrows; haemocytes (dotted arrows). H) Altered follicle (af) with haemocyte infiltration (*). I) Patch of inflammatory tissue (*). Atretic oocyte (arrow). J) Haemocytes (dotted arrow) infiltrated among hyperthrophic adipogranular cells (adg). K) Oocytes with anomalous cortical areas (arrows). Notice the regular nuclear contour (n). L) Group of oocytes with indented nuclei (dotted arrows), dense chromatin patches (arrows). Nucleus (n), nucleolus (nu). M) Oocyte with a dense cytosolic net of threads (*). Nucleus (n). N-O) Oocytes showing dense cytosolic filaments (arrows). Indented nucleus (dotted arrow), adipogranular cells (adg). Haemalum - eosin staining (A-I, L, N-O); trichrome staining of Galgano (J, M). Bars: 100 μm (A-C); 50 μm (E-I); 25 μm (J); 10 μm (D, K-O). P) Table reporting the frequencies (in %) of the observed alterations in ovarian anatomy.

significant alterations in the cytoskeletal structure and, in particular, the formation of a net of dense threads (Fig. 5N and O).

3.6. Effect of MNP on carbohydrate residue distribution

In all specimens exposed to MNP, significant alterations in carbohydrate distribution were consistently observed in the oocytes and adipogranular cells (Fig. 6). In controls, staining with fluorescent lectins showed that mannose, fucose, and glcNAc localised in the zona pellucida and in small cortical granules (Fig. 6A–A1). Notable labelling was also observed on scattered granules of adipogranular cells (Fig. 6B, B1).

Following MP exposure, mannose was dispersed in the oocyte cytoplasm (Fig. 6A–A2), and fucose disappeared (Fig. 6A–A3). At the same time, glcNAc did not change localisation compared with controls (Fig. 6A–A1). Adipogranular cells (Fig. 6B) exhibited cytosolic granules positive to negative for mannose and fucose and negative for glcNAc (Fig. 6B1-B2). Exposure to NPs apparently did not induce significant changes in labelling localisation in oocytes (Fig. 6A–A1). In adipogranular cells (Fig. 6B), mannose and fucose did not change localisation (Fig. 6B1), while glcNAc positivity disappeared on day 11 (Fig. 6B2).

Quantification of fluorescence showed that, in addition to changes in localisation, labelling intensity also varied. Compared with control oocytes, MPs (Fig. 6A4, A5) reduced mannose, fucose, and GlcNAc, regardless of whether they were cortical or cytosolic. NPs, on the other hand, decreased these three sugars at day 3 (Fig. 6A4) but exhibited different effects on day 11, since increased mannose and decreased fucose and glcNAc (Fig. 6A5). In adipogranular cells (Fig. 6B3, B4), MPs consistently reduced fluorescence intensity. In contrast, NPs reduced mannose and GlcNAc but increased fucose.

3.7. Effect of MNP exposure on collagen distribution

In control specimens (Fig. 7A–A1), no matter the day of treatment, collagen formed a fine meshwork surrounding the follicles and the adipogranular and vesicular cells.

In mussels exposed to MPs (Fig. 7B, B1) but above all to NPs (Fig. 7C, C1), collagen fibres were denser, more compact, especially on day 11. Fluorescence quantification (Fig. 7D–F) confirmed the cytological evidence.

4. Discussion

The present study shows that exposure to MNPs induces significant oxidative stress in ovaries, confirming previous findings in the gonads of different species (Wang et al., 2019; Wu et al., 2025) and in tissues (Romano et al., 2025a).

Unexpectedly, no significant differences were observed in ROS and lipid peroxides between exposures to MPs and NPs. This apparently contrasts with the notion that toxicity increases while particle size decreases. Small particles easily penetrate cells (Shi et al., 2025) and, by exposing a larger surface area, release large quantities of leachate. Polystyrene MNPs, in fact, release phthalates and bisphenols (Gulizia et al., 2023) and volatile organic compounds (Beel et al., 2023), such as xylene, benzene, and benzaldehyde, pro-oxidants interfering with the female reproductive system (Suaidi et al., 2022). Polystyrene also releases substantial amounts of styrene (Motta et al., 2025), another

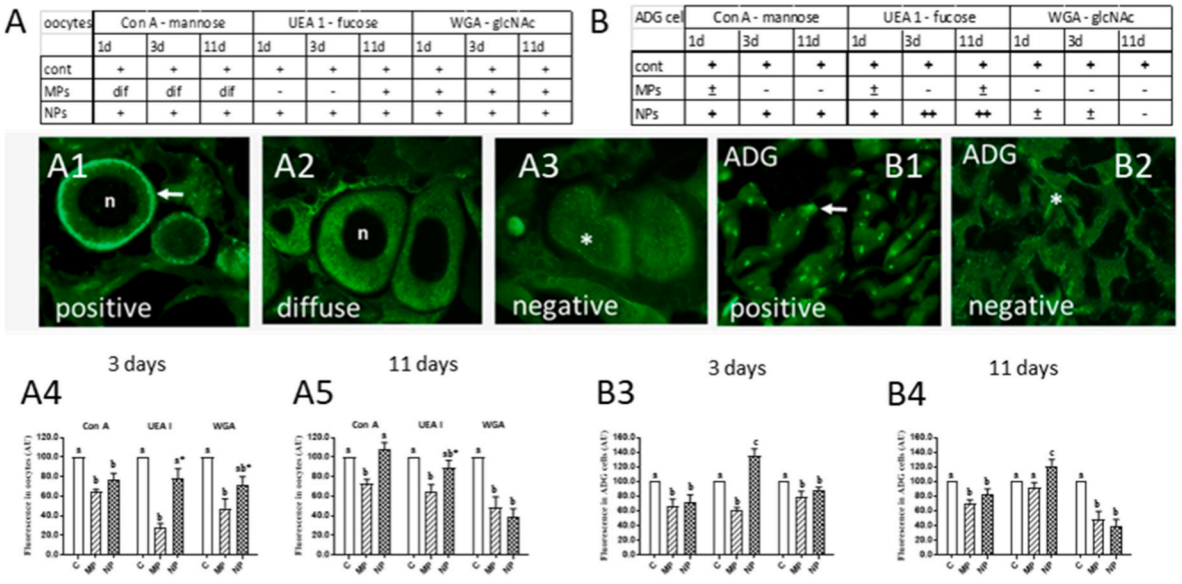

Fig. 6. Effects of MPs and NPs exposure for 1, 3, or 11 days on the presence and distribution of mannose, fucose, and N-Acetyl glucosamine in ovaries. Table (A-B) and representative images (A1-B2) showing fluorescence localisation in oocytes (A1-A3) and adipogranular cells (B1-B2). Quantification of fluorescence intensity in oocytes (A4-A5) and adipogranular cells (B3-B4). Staining with FITC-labeled lectins Con A, UEA I, and WGA. Fluorescence quantifications; values are means ± SD, obtained using ImageJ (free version 1.54p, updated 17 February 2025). Different letters indicate statistically significant differences determined by one-way ANOVA ($p < 0.05$). Asterisks (*) denote significant differences according to Student's t-test ($p < 0.05$).

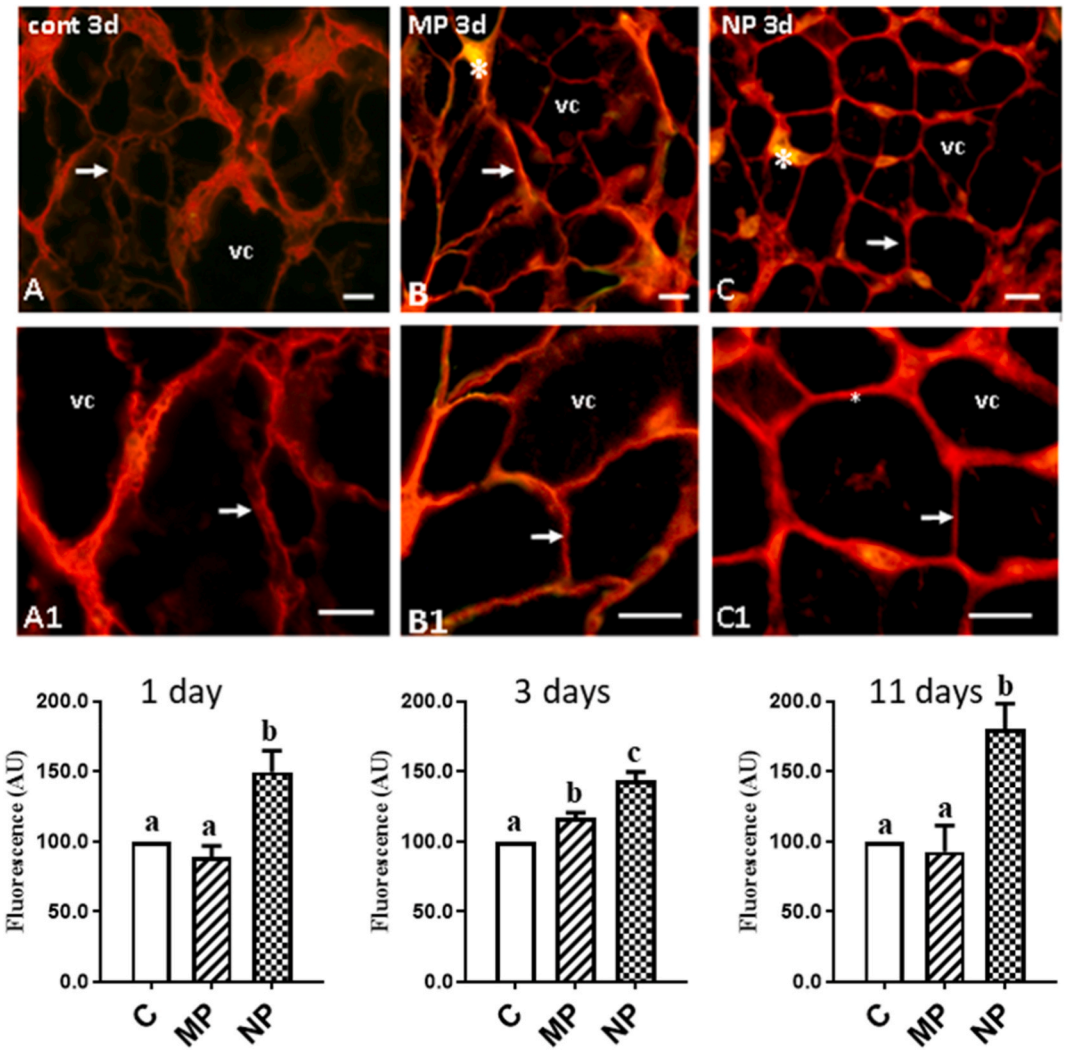

Fig. 7. Mantle fibrosis in mussels exposed to MPs or NPs for 1, 3 or 11 days. A-C1) Representative images showing the distribution of collagen fibres. Collagen (arrows) surrounds vesicular (vc) and adipogranular (*) cells. Notice the moderate (B) and significantly (C) compacted fibres in exposed samples. Picrosirius Red staining observed under UV light. Scale bars: 50 μm. (D-F) Fluorescence quantifications; values are means ± SD, obtained using ImageJ (free version 1.54p, updated 17 February 2025). Different letters indicate statistically significant differences determined by one-way ANOVA ($p < 0.05$). (For interpretation of the references to colour in this figure legend, the reader is referred to the Web version of this article.)

pro-oxidant that affects reproduction (Brown et al., 2000). In the experiments conducted, the NPs are 220-fold more numerous than MPs but 50 times smaller, thereby exposing a surface approximately 10 times smaller.

Another possible explanation for this result is that the more intense insult caused by NPs activated stronger defence mechanisms, as indicated by SOD2 upregulation on day 1 (Zaidi et al., 2021). The downregulation observed in the 3- and 11-day samples, however, contradicts the hypothesis, indicating that the effect, if present, was temporary. SOD2 is a mitochondrial enzyme, primarily detoxifying superoxide, whose activity depends on cell context, signal transduction, and transcription factors (NF-κB, Nrf2, FoxO; Ghantabpour et al., 2025). Additionally, it should not be forgotten that mussel oocytes contain ovothiol, a non-enzymatic antioxidant that scavenges H2O2 radicals (Diaz de Cerio et al., 2020). Therefore, further in-depth investigations are required to fully understand the roles of various pro- and antioxidants.

Oxidative stress damages DNA and, consequently, impairs protein synthesis and repair (Tang, 2025). In mussel ovaries, this cytotoxic effect was evidenced by changes in the protein pattern, with several bands up- or downregulated on gels. Results support previous evidence that polystyrene alters protein profiles, hindering oogenesis and energy metabolism (Gonçalves et al., 2025). Currently, the only proteins whose changes were quantified by Western Blot are the cytoskeletal vinculin and tubulin. The former acts as an adapter, an intermediate filament that anchors actin filaments to the plasma membrane, and is crucial for cell cycle progression (Ochoa et al., 2024). The latter forms microtubules, which are responsible for spindle formation, and are disrupted by oxidative stress (Wuri et al., 2023).

Staining with fluorescent phalloidin confirmed that alterations in vinculin and tubulin expression were associated with a partial disruption of the actin cytoskeleton. In control oocytes, actin is concentrated in the cortical cytoplasm, and around the yolk platelets and the cortical alveoli (Becker & Hart, 1996). Particularly after exposure to NPs, this organisation was lost, leading to redistribution throughout the entire cytoplasm. The disorganisation of the cytoskeleton is also evident at the morphological level. In histological preparations, staining revealed a time-dependent appearance of a dense filamentous net in the oocyte cytoplasm. Similar retraction and aggregation or collapse of intermediate filaments toward the cell interior have been described after exposure to toxins (Wickstrom et al., 1995). Although no conclusion can be reached, it is relevant to consider that intermediate filaments are critical for proper cell and tissue homeostasis and for stress responses

(Pérez-Sala & Quinlan, 2024).

The extensive damage to cytoskeletal organisation would significantly interfere with oocyte structure and function (Tatíčková et al., 2023), particularly oogonial proliferation. Mitosis, in fact, requires tubulins for the mitotic spindle and actin for the contractile ring that separates the two sister cells during cytokinesis. Immunocytochemical investigations indicate that PCNA-positive nuclei in oogonia and early-growing oocytes are markedly reduced in number, especially in samples exposed to NPs.

The altered cytoskeleton also explains the oocytes with indented nuclear contours. Shape is maintained by the nucleoskeleton and the nuclear lamina, in particular, whose major component is another intermediate filament, the lamins. The lamina contributes to maintaining nuclear integrity and function (Patil & Sengupta, 2021), including DNA repair and replication (Pu et al., 2021).

Oxidative stress (Giannessi et al., 2025) and cytoskeletal anomalies (Solomon et al., 2022) would account for the increased number of degenerating oocytes. Oocyte selection occurs via apoptosis to prevent inflammation and facilitate recovery of materials (Haanen & Vermes, 1995). The activation of apoptosis in mussel ovaries is demonstrated by the increased caspase 3 activity and BAK expression. However, the dispersion of waste materials in the follicle lumen suggests that other degenerative processes were activated. Ferroptosis is a possibility, as it is associated with high levels of oxidative stress and lipid peroxidation (Zhou et al., 2025) and, more importantly, determines plasma membrane rupture (Han et al., 2025). The evidence of inflammation, on the other hand, supports the onset of pyroptosis (Hou et al., 2021). The presence of the relative markers is under investigation.

Staining with picrosirius red confirmed the onset of inflammation, as it showed moderate but significant fibrosis (Ramos-Tovar & Muriel, 2020). The consequences of collagen fibre compaction remain uncertain, but increased stiffness of the mantle connective tissue might affect the mechanical and trophic support for the ovarian tissue. Significant that ovarian stiffness in mammals has been associated with ovarian ageing (Zaniker et al., 2024). At the molecular level, ovarian fibrosis has been associated with the activation of the WNT/β-catenin and TGF-β/Smad pathways (Cen et al., 2025). Both regulate cell proliferation, differentiation and tissue homeostasis, and control follicular development. Fibrosis, therefore, contributed to the observed impairment of oocyte quality (Harwood et al., 2008; Ji et al., 2023).

PAS staining of gels and lectin-based analyses provided additional insights into the impact of MNPs on mussel oogenesis. Marked effects on protein glycosylation patterns were observed, suggesting modifications in post-translational pathways. *Lectin staining* confirmed the presence of mannose, fucose, and glcNAc residues in the oocytes (Motta et al., 2021; Rosati et al., 2023) and highlighted significant variations in MNPs-treated samples. The exact consequence of such variations is not clear at the moment. However, fucose and mannose are essential in egg interaction with the sperm (Macedo et al., 2007), while glcNAc, a component of hyaluronan, has putative roles in providing structure to the egg extracellular matrix (Magerd et al., 2022). As a cytoplasmic component, glcNAc is involved in oocyte maturation and ageing (Li et al., 2024) and controls reactive oxygen species levels, cortical granule exocytosis, and early embryonic development (Lee et al., 2021).

Alterations in carbohydrate composition were also detected in adipogranular cells, which provide nutritive support to developing oocytes (Berthelin et al., 2000). This implies a possible impairment of the reserve storage process and consequent impact on embryo development. Conversely, vesicular cells remained unaffected, in agreement with their role in storing glucose in inactive forms (Lenoir et al., 1989). Taken together with the oocyte structural damages, this evidence suggests reduced fecundity, as already reported, for example, in fish (Wang et al., 2019), molluscs (Kumari et al., 2023) and copepods (Kim et al., 2022).

5. Conclusion

In conclusion, the data suggests that both MPs and NPs have rapid, complex effects on the ovary of *Mytilus galloprovincialis*. Oxidative stress damages the cytoskeleton and alters protein expression and glycosylation patterns, leading to oocyte dysfunction with unpredictable consequences on fertilisation and embryo development.

Interestingly, no significant difference was observed in responses to MPs and NPs, despite the differences in particle size and concentration. This clearly indicates that further investigations are required to fully evaluate the toxicokinetics and toxicodynamics of MNPs. In particular, it is essential to deepen our understanding of the endocrine-disruptive effects and to clarify the molecular pathways involved in the observed cellular alterations.

Both aspects are highly relevant, as toxicants that affect oogenesis compromise the stability of natural environments. Mussel beds stabilise coastal substrates and provide sheltered niches for adults and larvae of many species. A decline in their abundance will seriously threaten the resilience of these ecosystems. There are also expected consequences at commercial levels, as mussels are among the most traded aquatic species. Overall, these considerations highlight the need for further investigation and prompt the development of intervention and mitigation strategies to reduce MNPs contamination.

Funding

This work was supported by the Ministero dell'Istruzione, dellUniversita'e della Ricerca (grant number 2024YRYS5 006; Finanziamento delle attivita' di base di ricerca (FFABR) MIUR art.1, comma 295, Legge 11/12/2016 n 232.

CRediT authorship contribution statement

Rossana Romano: Writing – review & editing, Writing – original draft, Visualization, Validation, Methodology, Investigation, Formal analysis, Data curation. **Vincenzo Migliaccio:** Writing – review & editing, Writing – original draft, Visualization, Validation, Software, Methodology, Investigation, Formal analysis, Data curation. **Chiara Maria Motta:** Writing – review & editing, Writing – original draft, Visualization, Validation, Resources, Investigation, Funding acquisition, Formal analysis, Data curation. **Luigi Rosati:** Writing – review & editing, Writing – original draft, Methodology, Investigation, Formal analysis. **Antonia Acquisto:** Methodology, Investigation. **Lillà Lionetti:** Writing – review & editing, Writing – original draft, Resources, Investigation. **Palma Simoniello:** Writing – review & editing, Writing – original draft, Visualization, Validation, Supervision, Methodology, Investigation, Funding acquisition, Formal analysis, Data curation, Conceptualization.

Declaration of competing interest

All authors disclose any financial or personal relationships that may be perceived as influencing their work.

Appendix A. Supplementary data

Supplementary data to this article can be found online at https://doi.org/10.1016/j.envpol.2026.128160.

Data availability

Data will be made available on request.

References

Agnese, M., Verderame, M., De Meo, E., Prisco, M., Rosati, L., Limatola, E., Del Gaudio, R., Aceto, S., Andreuccetti, P., 2013. A network system for vitellogenin synthesis in the mussel *Mytilus galloprovincialis* (L.). J. Cell Physiol 228 (3), 547–555. https://doi.org/10.1002/jcp.24161.

Aguilar Díaz De León, J., Borges, C.R., 2020. Evaluation of oxidative stress in biological samples using the thiobarbituric acid reactive substances assay. JoVE J. 159. https://doi.org/10.3791/61122, 10.3791/61122.

An, R., Wang, X., Yang, L., Zhang, J., Wang, N., Xu, F., Hou, Y., Zang, H., Zhang, L., 2021. Polystyrene microplastics cause granulosa cells apoptosis and fibrosis in ovary through oxidative stress in rats. Toxicology 449, 152665.

Balali, H., Morabbi, A., Karimian, M., 2024. Concerning influences of micro/nano plastics on female reproductive health: focusing on cellular and molecular pathways from animal models to human studies. Reprod. Biol. Endocrinol. 22, 141. https://doi.org/10.1186/s12958-024-01314-7.

Becker, K.A., Hart, N.H., 1996. The cortical actin cytoskeleton of unactivated zebrafish eggs: spatial organization and distribution of filamentous actin, nonfilamentous actin, and myosin-II. Mol. Reprod. Dev. 43 (4), 536–547. https://doi.org/10.1002/(SICI)1098-2795(199604)43:4%3C536::AID-MRD17%3E3.0.CO;2-X.

Beel, G., Langford, B., Carslaw, N., Shaw, D., Cowan, N., 2023. Temperature-driven variations in VOC emissions from plastic products and their fate indoors: a chamber experiment and modelling study. Sci. Total Environ. 881, 163497. https://doi.org/10.1016/j.scitotenv.2023.163497.

Berthelin, C., Kellner, K., Mathieu, M., 2000. Histological characterization and glucose incorporation into glycogen of the Pacific oyster *Crassostrea gigas* storage cells. Mar. Biotechnol. 2 (2), 136–145. https://doi.org/10.1007/s101269900017.

Brown, N.A., Lamb, J.C., Brown, S.M., Neal, B.H., 2000. A review of the developmental and reproductive toxicity of styrene. Regul. Toxicol. Pharmacol. 32 (3), 228–247. https://doi.org/10.1006/rtph.2000.1406.

Capolupo, M., Valbonesi, P., Fabbri, E., 2021. A comparative assessment of the chronic effects of micro- and nano-plastics on the physiology of the mediterranean mussel *Mytilus galloprovincialis*. Nanomaterials 11 (3), 649. https://doi.org/10.3390/nano11030649.

Cen, Z., Lv, S., Li, Q., Zhang, J., Mei, S., Hu, X., Yang, A., 2025. Acute exposure to antimony elicits endocrine disturbances, leading to PCOS and ovarian fibrosis in female zebrafish. Comp. Biochem. Physiol. C Toxicol. Pharmacol. 294, 110198. https://doi.org/10.1016/j.cbpc.2025.110198.

Contino, M., Ferruggia, G., Indelicato, S., Pecoraro, R., Scalisi, E.M., Salvaggio, A., Brundo, M.V., 2023. Polystyrene nanoplastics in aquatic microenvironments affect sperm metabolism and fertilization of *Mytilus galloprovincialis* (Lamarck, 1819). Toxics 11 (11), 924. https://doi.org/10.3390/toxics11110924.

Diaz de Cerio, O., Reina, L., Squatrito, V., Etxebarria, N., Gonzalez-Gaya, B., Cancio, I., 2020. Gametogenesis-related fluctuations in ovothiol levels in the mantle of mussels from different estuaries: fighting oxidative stress for spawning in polluted waters. Biomolecules 10 (3), 373. https://doi.org/10.3390/biom10030373.

Donkers, J.M., Höppener, E.M., Grigoriev, I., Will, L., Melgert, B.N., van de Steed, E., Kooter, I.M., 2022. Advanced epithelial lung and gut barrier models demonstrate passage of microplastic particles. Micropl. Nanopl. 2, 6. https://doi.org/10.1186/s43591-021-00024-w.

Driver, A.S., Kodavanti, P.R., Mundy, W.R., 2000. Age-related changes in reactive oxygen species production in rat brain homogenates. Neurotoxicol Teratol 22, 175–181. https://doi.org/10.1016/S0892-0362(99)00069-0.

Ernhofer, B., Spittler, A., Ferk, F., Mišík, M., Zylka, M.M., Glatt, L., Boettiger, K., Solta, A., Kirchhofer, D., Timelthaler, G., Megyesfalvi, Z., Kopatz, V., Kovar, H., Knasmueller, S., Aigner, C., Kenner, L., Döme, B., Schelch, K., 2025. Small particles, big problems: polystyrene nanoparticles induce DNA damage, oxidative stress, migration, and mitogenic pathways predominantly in non-malignant lung cells. J. Hazard Mater. 495, 139129. https://doi.org/10.1016/j.jhazmat.2025.139129.

Fogliano, C., Carotenuto, R., Agnisola, C., Simoniello, P., Karam, M., Manfredonia, C., Avallone, B., Motta, C.M., 2023. Benzodiazepine delorazepam induces locomotory hyperactivity and alterations in pedal mucus texture in the freshwater gastropod *Planorbarius corneus*. Int. J. Mol. Sci. 24 (23), 17070. https://doi.org/10.3390/ijms242317070.

Gagné, F., Roubeau-Dumont, E., André, C., Auclair, J., 2023. Micro and nanoplastic contamination and its effects on freshwater mussels caged in an urban area. J. Xenobiotic 13 (4), 761–774. https://doi.org/10.3390/jox13040048.

Ghantabpour, T., Goudarzi, N., Parsaei, H., 2025. Overview of Nrf2 as a target in ovary and ovarian dysfunctions focusing on its antioxidant properties. J. Ovar. Res. 18 (1), 60. https://doi.org/10.1186/s13048-025-01639-w.

Giannessi, J., Pretti, C., Meucci, V., Intorre, L., De Marchi, L., Gabbrielli, B., Baratti, M., 2025. Biochemical and molecular stress responses to enrofloxacin in *Mytilus galloprovincialis*: transient or lasting effects? Aquat. Toxicol. 290, 107626. https://doi.org/10.1016/j.aquatox.2025.107626.

Gonçalves, J.M., Mendes, V.M., Manadas, B., Bebianno, M.J., 2025. Gender differences in protein expression after polystyrene nanoplastics exposure in mussels *Mytilus galloprovincialis*. Sci. Total Environ. 997, 180181. https://doi.org/10.1016/j.scitotenv.2025.180181.

Gulizia, A.M., Patel, K., Philippa, B., Motti, C.A., van Herwerden, L., Vamvounis, G., 2023. Understanding plasticiser leaching from polystyrene microplastics. Sci. Total Environ. 857, 159099. https://doi.org/10.1016/j.scitotenv.2022.159099.

Haanen, C., Vermes, I., 1995. Apoptosis and inflammation. Mediators Inflamm. 4(1), 5-15. org/10.1155/S0962935195000020.

Habumugisha, T., Zhang, Z., Uwizewe, C., Yan, C., Ndayishimiye, J.C., Rehman, A., Zhang, X., 2024. Toxicological review of micro- and nano-plastics in aquatic environments: risks to ecosystems, food web dynamics and human health. Ecotoxicol. Environ. Saf. 278, 116426. https://doi.org/10.1016/j.ecoenv.2024.116426.

Haddadi, A., Kessabi, K., Boughammoura, S., Rhouma, M.B., Mlouka, R., Banni, M., Messaoudi, I., 2022. Exposure to microplastics leads to a defective ovarian function and change in cytoskeleton protein expression in rat. Environ. Sci. Pol. 29 (23), 34594–34606. https://doi.org/10.1007/s11356-021-18218-3.

Han, S., Wei, Y., Wei, Y., et al., 2025. Mechanisms of programmed cell death in livestock follicular development and atresia: a review. J. Anim. Sci. Biotechnol. 16, 109. https://doi.org/10.1186/s40104-025-01241-6.

Harwood, B.N., Cross, S.K., Radford, E.E., Haac, B.E., De Vries, W.N., 2008. Members of the WNT signaling pathways are widely expressed in mouse ovaries, oocytes, and cleavage stage embryos. Dev. Dyn. 237 (4), 1099–1111. https://doi.org/10.1002/dvdy.21491DigitalObjectIdentifier.

Hou, J., Lei, Z., Cui, L., Hou, Y., Yang, L., An, R., Wang, Q., Li, S., Zhang, H., Zhang, L., 2021. Polystyrene microplastics lead to pyroptosis and apoptosis of ovarian granulosa cells via NLRP3/caspase-1 signaling pathway in rats. Ecotoxicol. Environ. Saf. 212, 112012. https://doi.org/10.1016/j.ecoenv.2021.112012.

Hu, M., Palić, D., 2020. Micro- and nano-plastics activation of oxidative and inflammatory adverse outcome pathways. Redox Biol. 37, 101620. https://doi.org/10.1016/j.redox.2020.101620.

Ji, J., Zhou, Y., Li, Z., Zhuang, J., Ze, Y., Hong, F., 2023. Impairment of ovarian follicular development caused by titanium dioxide nanoparticles exposure involved in the TGF-β/BMP/S mad pathway. Environ. Toxicol. 38 (1), 185–192. https://doi.org/10.1002/tox.23676.

Kim, K., Yoon, H., Choi, J.S., Jung, Y.J., Park, J.W., 2022. Chronic effects of nano and microplastics on reproduction and development of marine copepod *Tigriopus japonicus*. Ecotoxicol. Environ. Saf. 243, 113962. https://doi.org/10.1016/j.ecoenv.2022.113962.

Kumari, N., Samantaray, B.P., Patel, A., Kumar, R., 2023. Microplastics affect rates of locomotion and reproduction via dietary uptake in globally invasive snail *Physa acuta*. Water 15, 928. https://doi.org/10.3390/w15050928.

Lee, J., Kim, E., Hwang, S.U., Cai, L., Kim, M., Choi, H., Oh, D., Lee, E., Hyun, S.H., 2021. Effect of D-glucuronic acid and N-acetyl-D-glucosamine treatment during *in vitro* maturation on embryonic development after parthenogenesis and somatic cell nuclear transfer in pigs. Animals 11, 1034. https://doi.org/10.3390/ani11041034.

Lenoir, F., Robbins, I., Mathieu, M., Lubet, P., Gabbott, P.A., 1989. Isolation, characterization and glucose metabolism of glycogen cells (vesicular connective-tissue cells) from the labial palps of the marine mussel *Mytilus edulis*. Mar. Biol. 101, 495–501. https://doi.org/10.1007/BF00541651.

Leusch, F.D.L., Ziajahromi, S., 2021. Converting mg/L to particles/L: reconciling the occurrence and toxicity literature on microplastics. Environ. Sci. Technol. 55, 11470–11472. https://doi.org/10.1021/acs.est.1c04093.

Li, C., Qian, Z., Zhang, H., Ge, X., Chen, L., Xue, M., Tang, T., He, Z., Zheng, L., Cao, C., Zhang, K., Ma, R., Yao, B., 2024. O-GlcNAc participates in the meiosis of ageing oocytes by mediating mitochondrial function. Reproduction 168, e240138. https://doi.org/10.1530/REP-24-0138.

Lopez, G.L., Lamarre, A., 2025. The impact of micro- and nanoplastics on immune system development and functions: current knowledge and future directions. Reprod. Toxicol. 135, 108951. https://doi.org/10.1016/j.reprotox.2025.108951.

Macedo, N.M., Costa-Lotufo, L.V., Pessoa, C., Moraes, M.O., Bonfim, L.R., Ramos, M.V., 2007. Inhibition of sea urchin fertilization by plant lectins. Protein Pept. Lett. 14, 886–893. https://doi.org/10.2174/092986607782110356.

Magerd, S., Senarai, T., Thongsum, O., et al., 2022. Shrimp thrombospondin (TSP): presence of O-β1,4 N-acetylglucosamine polymers and its function in TSP chain association in egg extracellular matrix. Sci. Rep. 12, 7925. https://doi.org/10.1038/s41598-022-11873-7.

Migliaccio, V., Sica, R., Scudiero, R., Simoniello, P., Putti, R., Lionetti, L., 2019. Physiological adaptation to simultaneous chronic exposure to high-fat diet and dichlorodiphenyltrichloroethylene (DDE) in wistar rat testis. Cells 8 (5), 443. https://doi.org/10.3390/cells8050443.

Migliaccio, V., Di Gregorio, I., Penna, S., Panico, G., Lombardi, A., Lionetti, L., 2024. Adaptation of brown adipose tissue in response to chronic exposure to the environmental pollutant 1,1-Dichloro-2,2-bis(p-chlorophenyl) ethylene (DDE) and/or a high-fat diet in Male wistar rats. Nutrients 16, 2616. https://doi.org/10.3390/nu16162616.

Motta, C.M., Tammaro, S., Simoniello, P., Prisco, M., Ricchiari, L., Andreuccetti, P., Filosa, S., 2005. Characterisation of cortical alveoli content in several species of Antarctic notothenioids. J. Fish. Biol. 66 (2), 442–453. https://doi.org/10.1111/j.0022-1112.2005.00613.x.

Motta, C.M., Simoniello, P., Di Lorenzo, M., Migliaccio, V., Panzuto, R., Califano, E., Santovito, G., 2021. Endocrine-disrupting effects of copper and cadmium in the oocytes of the Antarctic emerald rockcod *Trematomus bernacchii*. Chemosphere 268, 129282. https://doi.org/10.1016/j.chemosphere.2020.129282.

Motta, C.M., Tizzano, M., Tagliafierro, A.M., Simoniello, P., Panzuto, R., Esposito, L., Migliaccio, V., Rosati, L., Avallone, B., 2018. Biocide triclosan impairs byssus formation in marine mussels *Mytilus galloprovincialis*. Environ. Pollut. 241, 388–396. https://doi.org/10.1016/j.envpol.2018.05.064.

Motta, C.M., Califano, E., Scudiero, R., Avallone, B., Fogliano, C., De Bonis, S., Raggio, A., Simoniello, P., 2022. Effects of cadmium exposure on gut villi in *Danio rerio*. Int. J. Mol. Sci. 23 (4), 1927. https://doi.org/10.3390/ijms23041927.

Motta, C.M., Fogliano, C., Trifuoggi, M., Toscanesi, M., Raggio, A., Di Marino, S., Venditti, P., Fasciolo, G., Avallone, B., Carotenuto, R., 2025. Polystyrene microplastic interferes with yolk reserve utilisation in early Artemia salina nauplii. Toxics 13 (8), 700. https://doi.org/10.3390/toxics13080700.

Motta, C.M., Rosati, L., Cretì, P., Montinari, M.R., Denre, P., Simoniello, P., Fogliano, C., Scudiero, R., Avallone, B., 2024. Histopathological effects of long-term exposure to

realistic concentrations of cadmium in the hepatopancreas of *Sparus aurata* juveniles. Aquat. Toxicol. 268, 106858. https://doi.org/10.1016/j.aquatox.2024.106858.
Ng, P.L., Kinn-Gurzo, S.S., Chan, K.Y.K., 2022. Microplastics impede larval urchin selective feeding. Sci. Total Environ. 838 (Pt 1), 155770. https://doi.org/10.1016/j.scitotenv.2022.155770.
Ochoa, A., Herrera, A., Menéndez, A., Estefanell, M., Ramos, C., Pons, S., 2024. Vinculin is required for interkinetic nuclear migration and cell cycle progression. J. Cell Biol. 223, e202106169. https://doi.org/10.1083/jcb.202106169.
Patil, S., Sengupta, K., 2021. Role of A- and B-type lamins in nuclear structure-function relationships. Biol. Cell 113, 295–310. https://doi.org/10.1111/boc.202000160.
Pellegrino, D., La Russa, D., Barberio, L., 2025. Pollution has no borders: microplastics in Antarctica. Environments 12 (3), 77. https://doi.org/10.3390/environments12030077.
Pérez-Sala, D., Quinlan, R.A., 2024. The redox-responsive roles of intermediate filaments in cellular stress detection, integration and mitigation. Curr. Opin. Cell Biol. 86, 102283. https://doi.org/10.1016/j.ceb.2023.102283.
Pu, W., Zhang, H., Qin, P., Deng, L., 2021. Nuclear envelope integrity, DNA replication, damage repair and genome stability. Genome Instab. Dis. 2, 102–114. https://doi.org/10.1007/s42764-021-00039-w.
Pujol, G., Marín-Gual, L., González-Rodelas, L., Álvarez-González, L., Chauvigné, F., Cerdà, J., Teles, M., Roher, N., Ruiz-Herrera, A., 2025. Short-term polystyrene nanoplastic exposure alters zebrafish germline and reproductive outcomes. J. Hazard Mater. 481, 136529. https://doi.org/10.1016/j.jhazmat.2024.136529.
Ramos-Tovar, E., Muriel, P., 2020. Molecular mechanisms that link oxidative stress, inflammation, and fibrosis in the liver. Antioxidants 9, 1279. https://doi.org/10.3390/antiox9121279.
Romano, R., Cocozza di Montanara, A., Sandulli, R., Simoniello, P., 2025b. Bibliometric analysis of research on nanoplastics (NPs): uptake, bioaccumulation, and cellular internalization in scientific literature. Environments 12 (11), 441. https://doi.org/10.3390/environments12110441.
Romano, R., Rosati, L., Napolitano, G., Ferrigno, F., Chianese, T., Motta, C.M., Simoniello, P., 2025a. Polystyrene micro and nanoplastics: a comparative study of the cytotoxic effects exerted on *Mytilus galloprovincialis* gills. Ecotoxicol. Environ. Saf. 302, 118683. https://doi.org/10.1016/j.ecoenv.2025.118683.
Rosati L, Agnese M, Abagnale L, Aniello F, Andreuccetti P, Prisco M. The Mussel Mytilus galloprovincialis in the Bay of Naples: New Insights on Oogenic Cycle and Its Hormonal Control. Anat Rec (Hoboken). 2019 Jun;302(6):1039-1049. doi: 10.1002/ar.24075. Epub 2019 Feb 22. PMID: 30730612.
Rosati, L., Chianese, T., De Gregorio, V., Verderame, M., Raggio, A., Motta, C.M., Scudiero, R., 2023. Glyphosate interference in follicular organization in the wall lizard *Podarcis siculus*. Int. J. Mol. Sci. 24, 7363. https://doi.org/10.3390/ijms24087363.
Schmidt, A., da Silva Brito, W.A., Singer, D., Mühl, M., Berner, J., Saadati, F., Wolf, C., Miebach, L., Wende, K., Bekeschus, S., 2023. Short-and long-term polystyrene nano- and microplastic exposure promotes oxidative stress and divergently affects skin cell architecture and wnt/beta-catenin signaling. Part. Fibre Toxicol. 20 (1), 3. https://doi.org/10.1186/s12989-023-00513-1.
Shi, X., Wang, X., Huang, R., Tang, C., Hu, C., Ning, P., Wang, F., 2022. Cytotoxicity and genotoxicity of polystyrene micro- and nanoplastics with different size and surface modification in A549 cells. Int. J. Nanomed. 17, 4509–4523. https://doi.org/10.2147/IJN.S381776.
Shi, Y., Jiao, K., Li, L.A., Guo, W., Abo-Raya, M.H., Lee, J.S., Amouri, R.E.L., Hu, H., Wang, Y., 2025. The stealthy journey of nanoplastics in bivalves: accumulation dynamics and toxic burden. Environ. Sci. Nano 12 (1), 4748–4767. https://doi.org/10.1039/D5EN00673B.
Simoniello, P., Filosa, S., Riggio, M., Scudiero, R., Tammaro, S., Trinchella, F., Motta, C. M., 2010. Responses to cadmium intoxication in the liver of the wall lizard *Podarcis sicula*. Comp. Biochem. Physiol. C Toxicol. Pharmacol. 151 (2), 194–203. https://doi.org/10.1016/j.cbpc.2009.10.005.
Solomon, T., Rajendran, M., Rostovtseva, T., Hool, L., 2022. How cytoskeletal proteins regulate mitochondrial energetics in cell physiology and diseases. Philos. Trans. R. Soc. B 377, 20210324. https://doi.org/10.1098/rstb.2021.0324.
Suaidi, N.A., Alshawsh, M.A., Hoe, S.Z., Mokhtar, M.H., Zin, S.R.M., 2022. Toxicological effects of technical xylene mixtures on the female reproductive system: a systematic review. Toxics 10, 235. https://doi.org/10.3390/toxics10050235.
Talbot, R., Chang, H., 2022. Microplastics in freshwater: a global review of factors affecting spatial and temporal variations. Environ. Pollut. 292 (Pt B), 118393. https://doi.org/10.1016/j.envpol.2021.118393.
Tang, K.H.D., 2025. Genotoxicity of microplastics on living organisms: effects on chromosomes, DNA and gene expression. Environments 12, 10. https://doi.org/10.3390/environments12010010.
Tatíčková, M., Trebichalská, Z., Kyjovská, D., Otevřel, P., Kloudová, S., Holubcová, Z., 2023. The ultrastructural nature of human oocytes' cytoplasmic abnormalities and the role of cytoskeleton dysfunction. F&S Sci 4, 267–278. https://doi.org/10.1016/j.xfss.2023.09.002.
Upendra, S., Kaur, J., 2023. Microplastic pollution in seawater: a review study. Nat. Environ. Pollut. Technol. 22 (3). https://doi.org/10.46488/NEPT.2023.v22i03.050.
Valdez-Cibrián, A., Kozak, E.R., Franco-Gordo, C., 2024. Microplastic ingestion in marine mesozooplankton species associated with functional feeding traits. Mar. Environ. Res. 200, 106650. https://doi.org/10.1016/j.marenvres.2024.106650.
Vroom, R.J.E., Koelmans, A.A., Besseling, E., Halsband, C., 2017. Ageing of microplastics promotes their ingestion by marine zooplankton. Environ. Pollut. 231 (Pt 1), 987–996. https://doi.org/10.1016/j.envpol.2017.08.088.
Wang, J., Li, Y., Lu, L., Zheng, M., Zhang, X., Tian, H., Wang, W., Ru, S., 2019. Polystyrene microplastics cause tissue damage, sex-specific reproductive disruption and transgenerational effects in marine medaka. Environ. Pollut. 254, 113024. https://doi.org/10.1016/j.envpol.2019.113024.
Weber, A., Jeckel, N., Weil, C., Umbach, S., Brennholt, N., Reifferscheid, G., Wagner, M., 2021. Ingestion and toxicity of polystyrene microplastics in freshwater bivalves. Environ. Toxicol. Chem. 40 (8), 2247–2260. https://doi.org/10.1002/etc.5076.
Wickstrom, M.L., Khan, S.A., Haschek, W.M., Wyman, J.F., Eriksson, J.E., Schaeffer, D.J., Beasley, V.R., 1995. Alterations in microtubules, intermediate filaments, and microfilaments induced by microcystin-LR in cultured cells. Toxicol. Pathol. 23, 326–337. https://doi.org/10.1177/019262339502300309.
Wu, D., Carter, L., Kay, P., Holden, J., Yin, Y., Guo, H., 2025. Female zebrafish are more affected than males under polystyrene microplastics exposure. J. Hazard Mater. 482, 136616. https://doi.org/10.1016/j.jhazmat.2024.136616.
Wuri, L., Burghardt, R.C., Arosh, J.A., Long, C.R., Banu, S.K., 2023. Hexavalent chromium disrupts oocyte development in rats by elevating oxidative stress, DNA double-strand breaks, microtubule disruption, and aberrant segregation of chromosomes. Int. J. Mol. Sci. 24, 10003. https://doi.org/10.3390/ijms241210003.
Xue, Y., Cheng, X., Ma, Z.Q., Wang, H.P., Zhou, C., Li, J., Zhang, D.L., Hu, L.L., Cui, Y.F., Huang, J., Luo, T., Zheng, L.P., 2024. Polystyrene nanoplastics induce apoptosis, autophagy, and steroidogenesis disruption in granulosa cells to reduce oocyte quality and fertility by inhibiting the PI3K/AKT pathway in female mice. J. Nanobiotechnol. 22 (1), 460. https://doi.org/10.1186/s12951-024-02735-7.
Yang, Z., DeLoid, G.M., Zarbl, H., Baw, J., Demokritou, P., 2023. Micro- and nanoplastics (MNPs) and their potential toxicological outcomes: state of science, knowledge gaps and research needs. NanoImpact 32, 100481. https://doi.org/10.1016/j.impact.2023.100481.
Yang, Z., Wang, J., 2025. From gonads to generations: mechanistic insights into reproductive disruption by polystyrene nanoplastics and co-contaminants in fish. Environ. Chem. Ecotoxicol. 1871–1883. https://doi.org/10.1016/j.enceco.2025.08.018.
Zaidi, S.K., Shen, W.J., Cortez, Y., Bittner, S., Bittner, A., Arshad, S., Huang, T.T., Kraemer, F.B., Azhar, S., 2021. SOD2 deficiency-induced oxidative stress attenuates steroidogenesis in mouse ovarian granulosa cells. Mol. Cell. Endocrinol. 519, 110888. https://doi.org/10.1016/j.mce.2020.110888.
Zaniker, E.J., Zhang, M., Hughes, L., La Follette, L., Atazhanova, T., Trofimchuk, A., Babayev, E., Duncan, F.E., 2024. Shear wave elastography to assess stiffness of the human ovary and other reproductive tissues across the reproductive lifespan in health and disease. Biol. Reprod. 110, 1100–1114. https://doi.org/10.1093/biolre/ioae050.
Zheng, Y., Li, J., Zhu, H., Hu, J., Sun, Y., Xu, G., 2025. Endocytosis, endoplasmic reticulum, actin cytoskeleton affected in tilapia liver under polystyrene microplastics and BDE153 acute co-exposure. Comp. Biochem. Physiol. C Toxicol. Pharmacol. 289, 110117. https://doi.org/10.1016/j.cbpc.2024.110117.
Zhou, J., Zhang, T., Lin, M., Wang, C., 2025. Mechanisms of follicular atresia: focus on apoptosis, autophagy, and ferroptosis. Front. Endocrinol.16, 1603467.doi.org/10.3389/fendo.2025.1603467.
Ziani, K., Ioniță-Mîndrican, C.B., Mititelu, M., Neacșu, S.M., Negrei, C., Moroșan, E., Drăgănescu, D., Preda, O.T., 2023. Microplastics: a real global threat for environment and food safety: a state-of-the-art review. Nutrients 15, 617. https://doi.org/10.3390/nu15030617.